Fundamental and Second-Harmonic Ultrasound Field Computation of Inhomogeneous Nonlinear Medium With a Generalized Angular Spectrum Method

François Varray, Alessandro Ramalli, Christian Cachard, Piero Tortoli, *Senior Member, IEEE*, and Olivier Basset

***Abstract*—The simulation of nonlinear propagation of ultrasound waves is typically based on the Kuznetsov-Zabolotskaya-Khokhlov equation. A set of simulators has been proposed in the literature but none of them takes into account a possible spatial 3-D variation of the nonlinear parameter in the investigated medium. This paper proposes a generalization of the angular spectrum method (GASM) including the spatial variation of the nonlinear parameter. The proposed method computes the evolution of the fundamental and second-harmonic waves in four dimensions (spatial 3-D and time). For validation purposes, the one-way fields produced by the GASM are first compared with those produced by established reference simulators and with experimental one-way fields in media with a homogeneous nonlinear parameter. The same simulations are repeated for media having an axial variation of the nonlinear parameter. The mean errors estimated in the focal region are less than 4.0% for the fundamental and 5.4% for the second harmonic in all cases. Finally, the fundamental and second-harmonic fields simulated for media having nonlinear parameter variations in the axial, lateral, and elevation directions, which cannot be simulated with other currently available methods, are presented. The new approach is also shown to yield a reduction in computation time by a factor of 13 with respect to the standard nonlinear simulator.**

I. Introduction

When an ultrasound (US) wave propagates, distortion of the wave induced by the medium appears, and harmonics of the transmitted frequency are created. The nonlinear behavior of the medium is exploited in medical applications because harmonic imaging and its extensions improve the quality of images in terms of axial and lateral resolution [1]. The increase in harmonics depends on the medium (density, sound velocity, and nonlinear parameter B/A), the initial pressure, and the propagation distance. The nonlinear parameter plays the main role in the distortion during the propagation. Experimental measurements have shown that pathological tissues present different nonlinear values than healthy tissues [2]. Classical values for the nonlinear parameter of tissues are in the range 5 to 11. When US contrast agents are involved, their nonlinear coefficient is very high compared with tissues [3]. The nonlinear parameter of a contrast agent can be greater than 50 depending on the concentration used. This property is exploited in harmonic imaging. Different methods estimate the nonlinear coefficient of a medium [4]. Ultrasound propagation in a nonlinear medium can be either experimentally tested or studied in simulation. However, specific tools are needed to simulate media with an inhomogeneous nonlinear coefficient, for instance, a vessel with contrast agents surrounded by tissue.

To compute the propagation of an ultrasound wave, different nonlinear simulation tools have been described in the literature for both focused and unfocused sources. Most of them are based on the well-known Kuznetsov-Zabolotskaya-Khokhlov (KZK) equation [5], [6], which takes into account the nonlinear effects, the absorption of the medium, and the diffraction of the probe. The probe and the medium parameters play an important role in the focalization of the transmitted energy and the complexity of the simulators is mainly dependent upon the probe diffraction function. Indeed, the diffraction computation is the longer step because of the correlation between the probe shape and the spatial discretization. Two approaches exist to compute the pressure propagation: the finite differences and the angular spectrum method (ASM). The former computes, step by step, the distortion of the initial waveform in the propagation plane. The ASM directly and quickly computes the waveform at the desired depth using an approach based on the Fourier transform (FT). This approach was initially introduced by Alais and Hennion [7]. Using the same strategy, Christopher and Parker [8], [9] proposed a new resolution scheme based on the discrete Hankel transform to implement the planar propagation of an US wave. Then Zemp *et al.* adapted this work and used the ASM to propose a new numerical solution [10]. The main simulators in nonlinear propagation used in the US community have been developed by Bernsten [11], Hamilton *et al.* [12], [13], and Voormolen [14] for the finite differences approach and by Varslot *et al.* [15], [16]

Manuscript received September 14, 2010; accepted May 4, 2011. Special thanks are due to ANR-07 TecSan-015-01 MONITHER for financial support. The main author is financially supported by the Franco-Italian University with a VINCI and a Gallilée grant and by the Rhone-Alpes region with an Explora'Doc grant.

F. Varray, A. Ramalli, C. Cachard, and O. Basset are with Université de Lyon, CREATIS; CNRS UMR 5220; INSERM U1044; INSA-Lyon; Université Lyon 1, Villeurbanne, France (e-mail: francois.varray@creatis.univ-lyon1.fr).

F. Varray, A. Ramalli, and P. Tortoli are with the Electronics and Telecommunications Department, Università degli Studi di Firenze, Firenze, Italy.

Digital Object Identifier 10.1109/TUFFC.2011.1956

and Yan and Hamilton [17] for the ASM. These simulators compute the waveform distortion in the entire space for axially symmetric sources. Recently, a new simulator to predict the complete 4-D acoustic field from arbitrary sources [18] has been proposed.

None of the techniques mentioned take into account the possible spatial variation of the nonlinear coefficient β. When complex media are simulated, such as media containing contrast agents, the evolution of the nonlinear coefficient is crucial. In this paper, we propose a generalization of the ASM (GASM) based on the mathematical background of Aanonsen *et al.* [19]. This GASM makes it possible to simulate propagation using the KZK equation with inhomogeneous nonlinear media.

The paper is organized as follows. The first part reviews the mathematical solutions for the first- and the second-harmonic propagation, using the ASM. Taking into account the spatial variations of the nonlinear coefficient, the generalization is then described. The second part presents simulations obtained with this new tool. First, the pressure fields in media with a homogeneous nonlinear coefficient are simulated and compared with those obtained with established simulators. Then GASM simulations of media with an inhomogeneous coefficient are presented. Experimental measurements are also shown, demonstrating GASM's high level of accuracy. Finally, the conclusions are presented.

II. The Mathematical Background of GASM

A. The Basis of ASM

The ASM is based on the FT of the pressure field $p(z,x,y,t)$ at a propagation distance z from the source. A 3-D hybrid FT must be used, corresponding to the superposition of a transverse 2-D FT in the lateral-elevation (x,y) plane and the temporal plane. These FTs of the function p are defined as

$$F_{xy}[p] = \iint p(x,y)e^{-i2\pi(f_x x + f_y y)}\mathrm{d}x\mathrm{d}y \tag{1}$$

$$F_t[p] = \int p(t)e^{i2\pi f_t t}\mathrm{d}t, \tag{2}$$

where f_x and f_y are the spatial frequencies in the x and y direction and f_t is the temporal frequency. Then, the final 3-D hybrid FT is obtained with

$$\mathcal{F}(p) = F_t[F_{xy}[p]]. \tag{3}$$

Using the same notations, the FT and the inverse Fourier transform (IFT) of the pressure are respectively expressed as

$$P(z,f_x,f_y,f_t) = \iiint p(z,x,y,t)e^{-i2\pi(f_x x + f_y y - f_t t)}\mathrm{d}x\mathrm{d}y\mathrm{d}t, \tag{4}$$

$$p(z,x,y,t) = \iiint P(z,f_x,f_y,f_t)e^{i2\pi(f_x x + f_y y - f_t t)}\mathrm{d}f_x\mathrm{d}f_y\mathrm{d}f_t. \tag{5}$$

From the definitions in (4) and (5), a property of the FT is obtained:

$$\mathcal{F}\left(\frac{\partial^n p}{\partial v^n}\right) = (-2i\pi f_v)^n \mathcal{F}(p) \tag{6}$$

$$\mathcal{F}\left(\frac{\partial^n p}{\partial t^n}\right) = (2i\pi f_t)^n \mathcal{F}(p), \tag{7}$$

where the variable v corresponds to x or y.

B. Propagation Equation

The propagation equation of a pressure wave $p(z,x,y,t)$ in a lossless medium is expressed as [19]

$$\left(\nabla^2 - \frac{1}{c_0^2}\frac{\partial^2}{\partial t^2}\right)p = -\frac{\beta}{\rho_0 c_0^4}\frac{\partial^2 p^2}{\partial t^2}, \tag{8}$$

where c_0 is the speed of sound, ρ_0 is the density, ∇ is the Laplacian, and β is the nonlinear coefficient related to the nonlinear parameter $\beta = 1 + B/2A$. The nonlinear coefficient is directly responsible for the increase of the harmonics in the propagation equation [20]. The Laplacian is expressed as

$$\nabla^2 p = \left(\frac{\partial^2}{\partial x^2} + \frac{\partial^2}{\partial y^2} + \frac{\partial^2}{\partial z^2}\right)p. \tag{9}$$

The pressure $p(z,x,y,t)$ can be defined as the sum of the harmonics p_i:

$$p = p_1 + p_2 + p_3 + \cdots + p_n. \tag{10}$$

The ASM can compute the fundamental, p_1, and second-harmonic, p_2, of the pressure wave at a given position. However, its use is based on the quasi-linear approximation, which states that $p_1 \gg p_2$ and that the higher harmonics are negligible. This approximation reduces the total pressure p to the sum of the fundamental and second-harmonic wave [17], [21]. Eq. (8) can be separated into two equations: the first one corresponds to the fundamental frequency f_0 and the second one to the second harmonic at $2f_0$ so that two classic propagation equations are obtained. These two equations allow p_1 and p_2 to be expressed as a function of the medium parameters:

$$\left(\nabla^2 - \frac{1}{c_0^2}\frac{\partial^2}{\partial t^2}\right)p_1 = 0 \tag{11}$$

$$\left(\nabla^2 - \frac{1}{c_0^2}\frac{\partial^2}{\partial t^2}\right)p_2 = -\frac{\beta}{\rho_0 c_0^4}\frac{\partial^2 p_1^2}{\partial t^2}. \tag{12}$$

C. Solution for the Fundamental Frequency

The 3-D FT of (11) and (12) is computed to obtain the pressure wave P_1 and P_2 in the Fourier domain. For the fundamental, using properties (6) and (7), (11) is changed to

$$4\pi^2(-f_x^2 - f_y^2)P_1 + \frac{4\pi^2 f_t^2}{c_0^2}P_1 + \frac{\mathrm{d}^2 P_1}{\mathrm{d}z^2} = 0. \quad (13)$$

It can be noted in (13) that the ratio $2\pi f_t/c_0$ is similar to the classic wave vector $k = 2\pi f_0/c_0$. Moreover, $2\pi f_x$ and $2\pi f_y$ are directly related to the x- and y-axis definition and can be assimilated to the wave vector on these axes. Using $k_t = 2\pi f_t/c_0$, $k_x = 2\pi f_x$, and $k_y = 2\pi f_y$, (13) can be rewritten as a classic harmonic oscillator differential equation:

$$\frac{\mathrm{d}^2 P_1}{\mathrm{d}z^2} + K^2 P_1 = 0, \quad (14)$$

where K is the 3-D k-vector that depends on the sampling frequencies in m^{-1}:

$$K(k_x, k_y, k_t) = \sqrt{k_t^2 - k_x^2 - k_y^2}. \quad (15)$$

Only the part in which K is real has been kept (i.e., $k_t^2 > k_x^2 + k_y^2$) because an imaginary K corresponds to evanescent waves, which can be ignored without loss of accuracy if the wave propagates longer than a few wavelengths [22]. In our case, this condition is considered to be respected.

The solution for the fundamental wave at each point (x, y, z) of the medium can be expressed from (14) as

$$p_1(z, x, y, t) = \mathcal{F}^{-1}\left(P_0(z_0, k_x, k_y, k_t)e^{-iK(z-z_0)}\right), \quad (16)$$

where P_0 is the 3-D FT of the source wave p_0 at the original position z_0. The final expression of the fundamental wave corresponds to a simple phase shift in the Fourier domain of the initial waveform. The matrix P_0 depends on the probe definition and the transmission strategy. Specific windows and signals can be used on the transducer because of its discretization. With an array transducer, specific apodization can also be selected on each element.

D. Solution for the Second-Harmonic Frequency

For the second-harmonic wave, the left part of (12) is solved in a procedure similar to that of the fundamental. When considering the FT of the right part, if the nonlinear parameter β is considered homogeneous in each direction, it can be removed from the integral in the FT and the resulting expression is similar to the one proposed by Du and Jensen [23]. Our contribution consists of considering the possible variations in the three spatial directions of the nonlinear parameter of the medium. The expression of the FT of the right part of (12) is developed as

$$\mathcal{F}\left(-\frac{\beta}{\rho_0 c_0^4}\frac{\partial^2 p_1^2}{\partial t^2}\right) = \frac{-1}{\rho_0 c_0^4}\mathcal{F}\left(\beta(x, y, z)\frac{\partial^2 p_1^2}{\partial t^2}\right). \quad (17)$$

Because the nonlinear parameter does not depend on time, the Fourier term of (17) can be rewritten as

$$\mathcal{F}\left(\beta\frac{\partial^2 p_1^2}{\partial t^2}\right) = \mathcal{F}\left(\frac{\partial^2 \beta p_1^2}{\partial t^2}\right) = -4\pi^2 f_t^2 \mathcal{F}(\beta p_1^2). \quad (18)$$

According to (18), the FT of (12) becomes

$$\frac{\mathrm{d}^2 P_2}{\mathrm{d}z^2} + K^2 P_2 = \frac{k_t^2}{\rho_0 c_0^2}\mathcal{F}(\beta p_1^2). \quad (19)$$

The solution to (19) is equivalent to solving, for each (k_x, k_y, k_t), a differential second-order equation in z with the general form:

$$\frac{\mathrm{d}^2 g(z)}{\mathrm{d}z^2} + K^2 g(z) = M(z). \quad (20)$$

After variation of the constant (see Appendix) and considering only the forward propagation, the inverse FT of P_2 is computed to obtain the final expression of the pressure wave $p_2(z, x, y, t)$:

$$p_2(z, x, y, t) = \mathcal{F}^{-1}\left(\frac{-i}{2K}\left(\int_{z_0}^{z} M(u, k_x, k_y, k_t)e^{iKu}\mathrm{d}u\right)e^{-iKz}\right) \quad (21)$$

with

$$M(z, k_x, k_y, k_t) = \frac{k_t^2}{\rho_0 c_0^2}\mathcal{F}(\beta(z, x, y)p_1(z, x, y, t)^2). \quad (22)$$

The formulation proposed in (21) allows the 3-D computation of the second-harmonic temporal wave propagating in media with an inhomogeneous nonlinear parameter in space.

E. Involvement of the Attenuation

The attenuation of acoustic media can be described by various laws [24]. In classic biological media, the attenuation is frequency-dependent and the K vector can be written [9], [24], [25] as

$$K_a = K - i\alpha(f_t), \quad (23)$$

where $\alpha(f_t)$ is the frequency-dependent attenuation. It is expressed as

$$\alpha(f_t) = \alpha_0\left(\frac{f_t}{1e6}\right)^{\gamma}, \quad (24)$$

where γ is a number between 1 and 2 for biological media that translates the frequency-dependent law, and α_0 is the attenuation constant of the medium in units of $\mathrm{Np{\cdot}m^{-1}{\cdot}MHz^{-\gamma}}$. To take into account the attenuation of the medium using the GASM, the previous expressions of p_1 and p_2 using the K vector must be updated by replacing K with K_a. If different absorption behaviors must be used, only this part must be updated to take into account the new law.

F. Computer Implementation

Eq. (16) and (21) were implemented using C language and the FT was performed using the FFTW library [26].

The accuracy and the calculation time of the simulations depend on the resolution considered in the spatial and temporal dimensions. For each Δz step, the evolution of the fundamental wave P_1 in 3-D (x, y, t) is computed, first in the Fourier domain and then in the temporal domain. It must be noted that the fundamental does not depend on the z sampling. With the temporal evolution of the fundamental, the matrix $M(z + \Delta z)$ could be computed. Then, to obtain the final evolution of the second-harmonic wave, an integral part, denoted I, must be computed. A classic finite difference method has been chosen to compute this integral. Thanks to the previous computed value at $M(z)$, the new value of the integral can be obtained by

$$\begin{aligned} I(z + \Delta z) &= \int_{z_0}^{z+\Delta z} M(u) e^{iKu} \mathrm{d}u \\ &= \int_{z_0}^{z} M(u) e^{iKu} \mathrm{d}u + \int_{z}^{z+\Delta z} M(u) e^{iKu} \mathrm{d}u. \end{aligned} \tag{25}$$

Then the iteration solution of (25) gives:

$$I(z + \Delta z) = I(z) + \frac{M(z + \Delta z) e^{iK(z+\Delta z)} + M(z) e^{iKz}}{2} \Delta z. \tag{26}$$

From (26), the final Fourier and temporal evolution of the second harmonic is easily computed from the two 3-D matrices $M(z)$ and $M(z + \Delta z)$. This integration step is the key point necessary to take into account the total 3-D inhomogeneous nonlinear parameter.

III. Results

A. Pressure-Wave Simulation in a Medium With a Homogeneous Nonlinear Parameter

The accuracy of the GASM is evaluated in comparison with two simulators used as the reference for a medium with a homogeneous nonlinear parameter. First, the well-known linear Field II simulator [27], [28] is used for the calculation of the pressure field at the fundamental frequency f. To compare the second-harmonic component, the finite difference Voormolen simulator [14] was chosen. This simulator, based on the KZK equation [5], [6], can calculate both the fundamental and the second-harmonic increase in the entire 3-D space. The one-way fields obtained with the GASM are compared with those obtained with Field II and with Voormolen's simulator. From the 4-D (3-D + t) data computed by the simulators, the maximal pressure is extracted at each 3-D point. In particular, the pressure values in the plane $y = 0$ were extracted and displayed in Figs. 1 and 2.

The probe parameters used for the simulations are summarized in Table I and correspond to a linear prototype array probe (Esaote S.p.A, Florence, Italy). A five-cycle 5-MHz sinusoidal tone burst weighted with a Gaussian function was transmitted on each elementary transducer with initial pressure p_0. All the simulations were conducted in a medium considered to be water with a homogeneous nonlinear parameter value of 3.5. The medium parameters used in the simulations are summarized in Table II. The resulting one-way fields are presented in Fig. 1 for the fundamental and in Fig. 2 for the second harmonic. The shape of the fundamental field calculated with the GASM is similar to both reference simulators. For the second harmonic, the GASM field is very close to the field obtained with the Voormolen simulator. In Fig. 1(c) and Fig. 2(b), the one-way pressure fields appear to contain noise. This noise exhibits a symmetric pattern along the z-axis and is a result of the numerical error in the FT of the discretization of the space used.

TABLE I. Parameters of the Probe Used in Simulation.

Parameter	Value
Pitch	245 μm
Kerf	30 μm
Height	6 mm
Number of elements	64
Transmit focus	70 mm
Elevation focus	23 mm
Peak pressure	100 kPa
α in Gaussian windows	2.5

TABLE II. Medium Characteristic Used in Simulation.

Parameter	Value
Density	1000 kg·m^{-3}
Speed of sound	1540 m·s^{-1}
Attenuation	0.025 Np·m^{-1}·MHz^{-2}
γ	2

To evaluate the accuracy of the GASM simulation, an error map was computed to compare the resulting one-way field with those obtained using the two reference simulators. The difference of the one-way fields was calculated and then normalized by dividing the values by the pressure at the focal point in the Voormolen simulator. The error is expressed as

$$\varepsilon_i = \frac{|p_i^{\text{Voormolen}} - p_i^{\text{GASM}}|}{\max(p_i^{\text{Voormolen}})} \tag{27}$$

with i equal to 1 or 2 when the error is evaluated for the fundamental or the second-harmonic one-way field, respectively. The resulting maps are presented in Fig. 3. In the focalization area of the field, defined by the −12-dB isoline around the focal point in the GASM and delimited by the dashed line, the maximum error, the mean error, and the standard deviation are computed for the two nonlinear propagation simulators. In Fig. 3(a), the difference obtained is 1.9% ± 1.3% with a peak of 8.5% inside the delimited surface. In Fig. 3(b), the difference is 1.9% ± 1.6% with a peak of 8.8%.

B. Pressure-Wave Simulation in a Medium With an Inhomogeneous Nonlinear Parameter

The GASM takes into account the variations of the nonlinear parameter by the integrative part of the variable

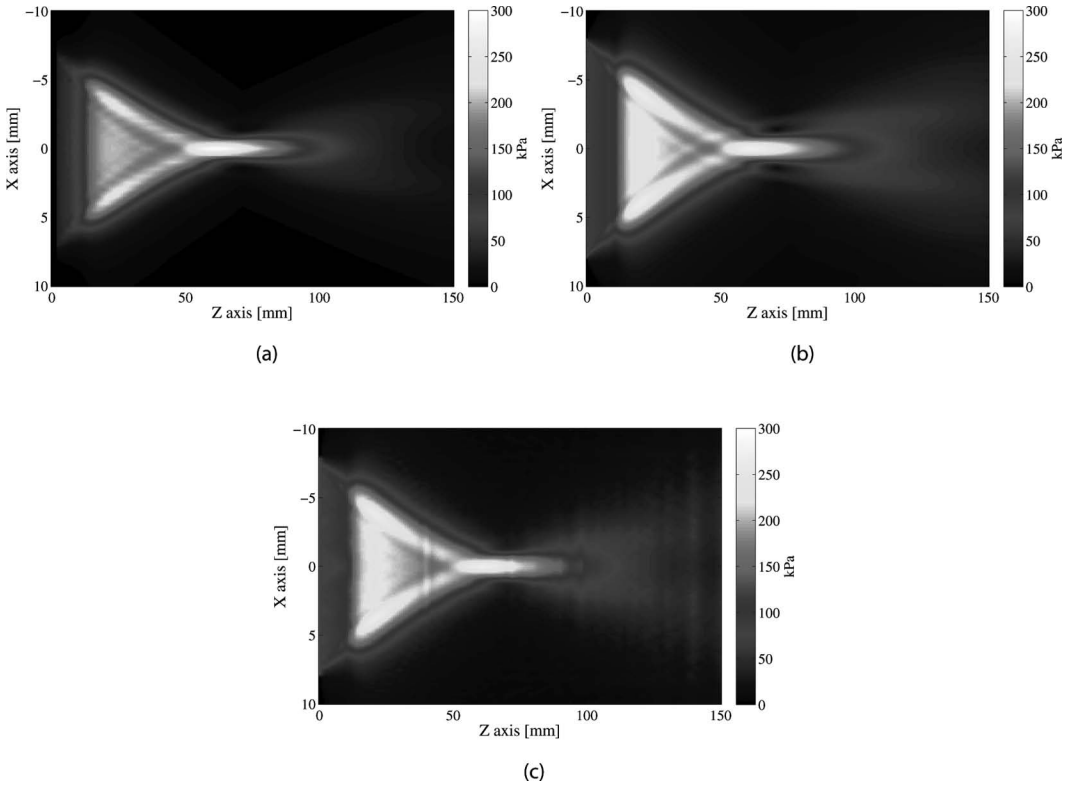

Fig. 1. One-way fundamental amplitude pressure fields obtained through (a) the Field II simulator, (b) the Voormolen simulator, and (c) the GASM simulator.

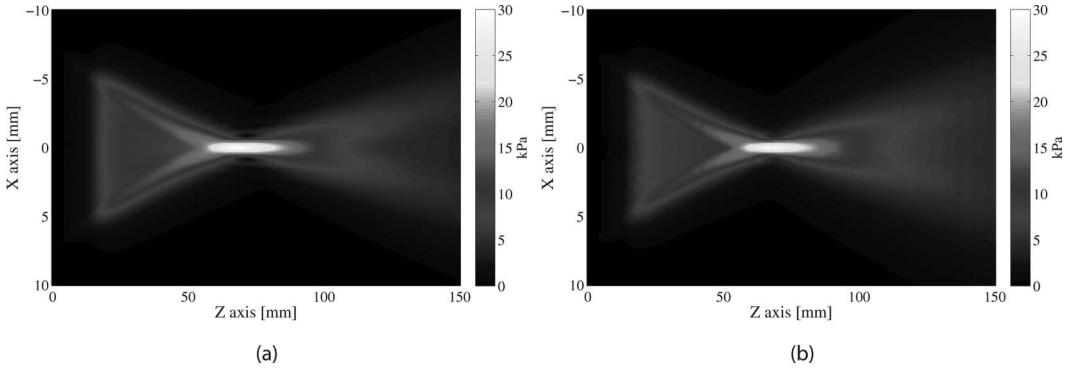

Fig. 2. One-way second-harmonic amplitude pressure fields obtained through (a) the Voormolen simulator and (b) the GASM. The pressure field obtained with the GASM is very close to the Voormolen pressure field.

$M(z, k_x, k_y, k_t)$ [see (22)]. With Voormolen's KZK simulator [14], it is possible to simulate a variation of the nonlinear parameter only along the z-axis. To compare the two simulators, we considered the case of a surrounding medium with a nonlinear parameter $\beta_1 = 3.5$ with an inclusion of a nonlinear parameter $\beta_2 = 7$. A linear slope of the nonlinear parameter's evolution was used at the interface of the two media to avoid a discontinuity [Fig. 4(a)]. The probe parameters of the transmitted signal are the same as the previous ones and are summarized in Table I. The resulting pressure profiles are presented in Fig. 4(b). The peak of the temporal response was computed along the z-axis of the probe with the GASM. Its evolution is very similar to that calculated with the Voormolen simulator. The error obtained for the second harmonic, when a medium with a homogeneous nonlinear parameter is considered, is 3.7% $\pm$ 1.9% with a peak error of 8.1%. When the inclusion is considered (inhomogeneous β), the error is 3.4% $\pm$ 2.2% with a peak error of 7.8%.

The GASM simulates more complex media, with 3-D variations of the nonlinear parameter, which cannot be simulated by the previously mentioned simulators. This property of the GASM is illustrated by two simulations. The first simulation is based on a phantom including two media disposed as follows: the upper region (corresponding to the negative x-axis) has a nonlinear parameter that is ten times greater than in the lower region. The resulting second-harmonic field obtained with the GASM is shown in Fig. 5(a). The pressure field is significantly different in the two regions. The amplitude of the second-harmonic component

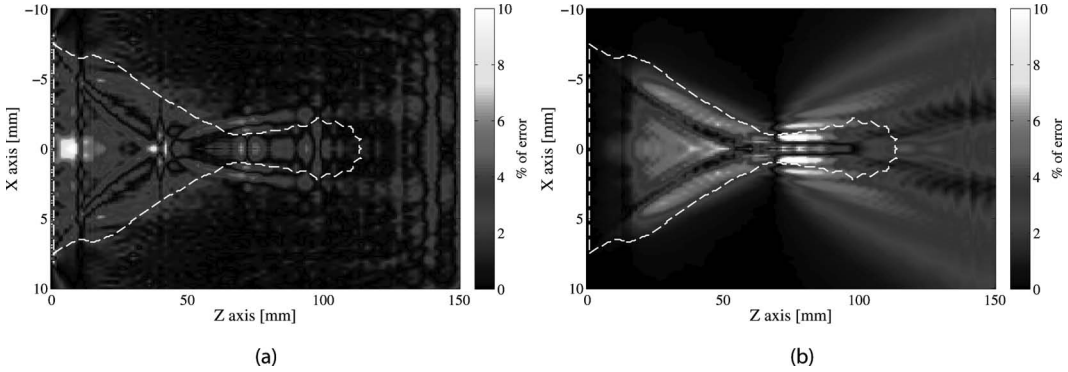

Fig. 3. Error map of the fundamental component of the GASM in comparison with (a) the Field II and (b) the Voormolen simulator. The dashed line is the −12-dB isoline and outlines the region where the error is considered. The pressure fields are normalized by the pressure obtained in the focal point.

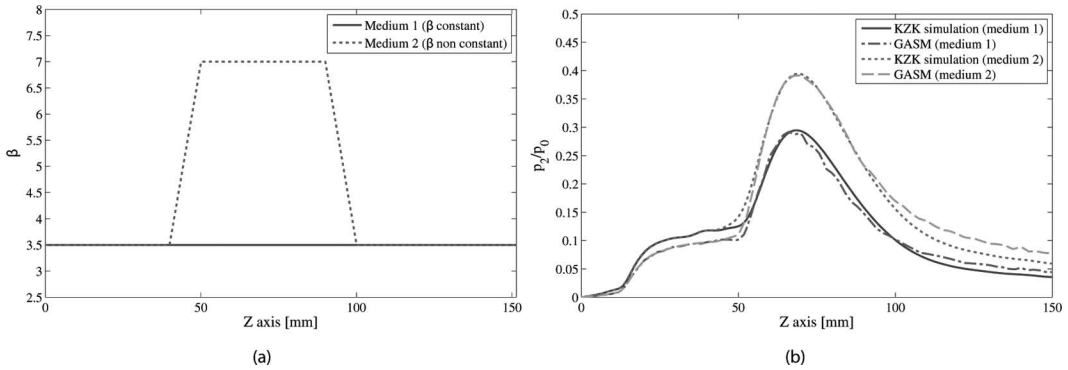

Fig. 4. (a) Profiles along the z-axis of the nonlinear parameter set in simulations; it is constant in medium 1 but not in medium 2. (b) Second-harmonic normalized pressure profile computed with the Voormolen and GASM simulators along the beam axis.

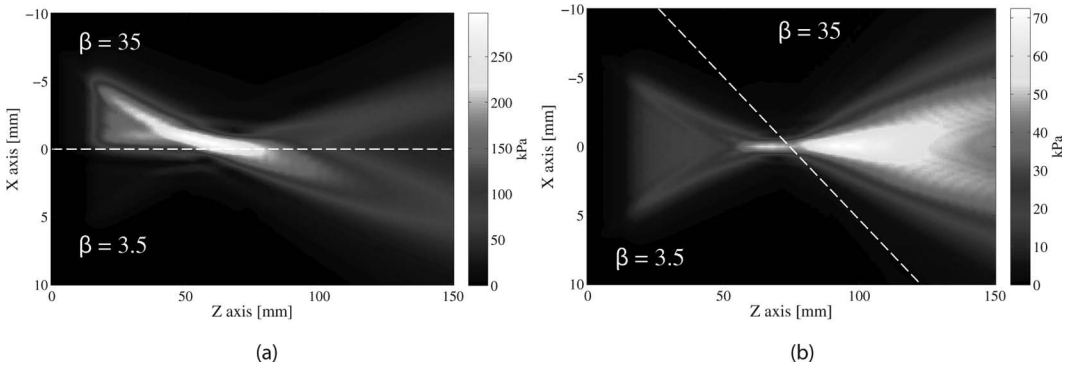

Fig. 5. One-way field of the second harmonic when the nonlinear parameter is not homogeneous in different directions of space. The dashed line separates the two different regions defined by the nonlinear parameter. Note that these simulations are not possible with the Voormolen and Field II simulators.

is larger in the area with higher nonlinear parameter and the peak is not centered on the probe axis. In the second simulation, the nonlinear parameter varies simultaneously along the x and z directions. The resulting second-harmonic image is shown in Fig. 5(b). This variation creates two focal points in the second-harmonic field: one at a position close to the focal point of the fundamental, and another one in the region where the nonlinearity increases sharply.

C. Experimental Measurements

To test the accuracy of the simulator, experimental acquisition of the fundamental and of the second-harmonic pressure fields was measured and compared with the simulation results. We repeated this test for two different transmission modalities. First, a conventional beam was considered. A five-cycle sine at 6.5 MHz with a Hanning window focused at 20 mm was transmitted. A Hanning apodization was also used on the active elements. Then a nonstandard transmission was used, requiring the application of specific apodization weights w_i to each element. A Bessel function apodization with respect to the x-axis was chosen [29]:

$$w_i = J_0(\alpha r_i), \tag{28}$$

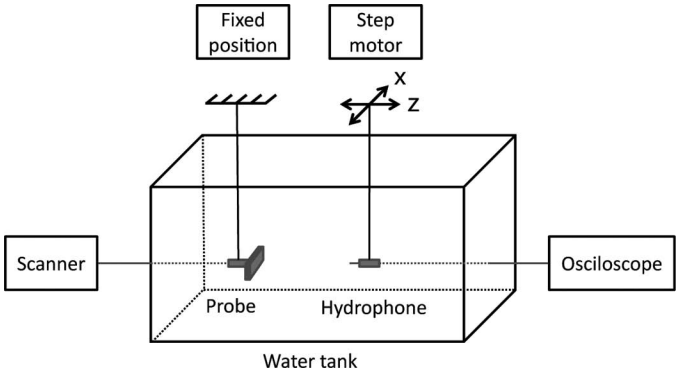

Fig. 6. Experimental setup.

where J_0 is the zero-order Bessel function, α is the spatial compression factor, and r_i is the distance between the active element and the center of the probe. To have the maximum intensity transmitted between 10 and 50 mm, an α value of 2100 m^{-1} was used. A five-cycle sine at 8 MHz with a Hanning window was transmitted. The scanner used was the ULA-OP system developed in the Microelectronics System Design Lab of the University of Florence [30] coupled with a prototype probe (Esaote S.p.A) whose parameters are summarized in Table I. Measurements were made in water, which has a nonlinear parameter of 3.5. A hydrophone (Marconi Materials Technology, Towcester, UK) recorded the pressure at different positions in the water tank with an accuracy of 0.8 mm in the z-direction and 0.2 mm in the x-direction. The experimental setup is illustrated in Fig. 6. The resulting experimental one-way fields are compared with those simulated by GASM in Fig. 7 for the focused beam and in Fig. 8 for the unfocused beam. The simulated fields show good agreement with the measurement for both the fundamental and second-harmonic components. The error maps of the fundamental and second-harmonic one-way fields were calculated as described previously using the −12-dB isoline around the focal point. The error value measurement is summarized in Table III. The large error peak observed in the second-harmonic field is localized in a very small area that is assumed to be an experimental artifact recorded during the experiment as a slight misalignment between the probe and the hydrophone. Because the signal is filtered around the fundamental and second harmonic components, higher harmonics did not degrade the quality of the result. Moreover, the third harmonic is merged in the experimental noise recorded by the hydrophone.

D. Computation Time

The computation time of nonlinear simulations is one of the most problematic points in nonlinear imaging [10], [18]. With the GASM, the computation time is greatly reduced by running it in the Fourier domain rather than finite difference approaches. The computation times of the two simulators, for the results displayed in Fig. 1, are shown in Table IV; the GASM is about 13 times faster.

TABLE III. Error Between GASM Simulations and Experimental Measure for a Focused and Unfocused Beam.

		Mean error (%)	Standard deviation (%)	Peak error (%)
Focused beam	p_1	5.4	2.7	14.5
	p_2	6.7	5.3	24.8
Unfocused beam	p_1	6.1	3.8	18.2
	p_2	5.8	4.6	30.7

TABLE IV. Computation Time of the KZK Simulator and the GASM.

	Voormolen simulator	GASM
Number of points in space (x, y, z, t)	$(303, 60, 390, 507)$	$(128, 64, 51, 512)$
Computation time	13 min 04 s	58 s

Results were obtained on an Intel Core 2 duo T9400 working at 2.53 GHz with 3.48 GB of memory (Intel Corp., Santa Clara, CA).

The difference in computation time comes from the number of points required in the different simulators. The finite difference method needs a large spatial sampling to obtain sufficient accuracy, particularly in the near field, for both the fundamental and the second harmonic. With the GASM, the fundamental does not depend on the z sampling. For the second harmonic, even if few points are presented in the discretization, the integration procedure involved in the calculation provides accurate results. Fewer sampling points are necessary for the simulation than those needed for the finite differences method to obtain comparable results.

IV. Discussion and Conclusions

The GASM is a new nonlinear US simulator that takes into account the diffraction of the probe as well as the nonlinearity and attenuation of the media. The first step of the GASM is to compute the FT of the probe geometry and the FT of the transmitted signal P_0 [see (16)]. The P_0 matrix takes into consideration all the probe parameters (geometry, frequency, probe shape) with the spatial and temporal discretization chosen in the simulation. This initialization defines all fields obtained with the GASM.

We have shown that, for a homogeneous nonlinear parameter, the GASM's performance is comparable to that of Field II for the fundamental or to that of the Voormolen finite difference simulator. This is illustrated by the error maps where no significant differences are observed between the GASM and the other simulators. The major contribution of the GASM is the possibility of simulating complex and arbitrary media in terms of nonlinearity. Indeed, the GASM can simulate complicated media with variations along the axial (z), lateral (x), and elevational (y) dimensions. The previous KZK simulator simulates the propagation wave along a stack of layers with different

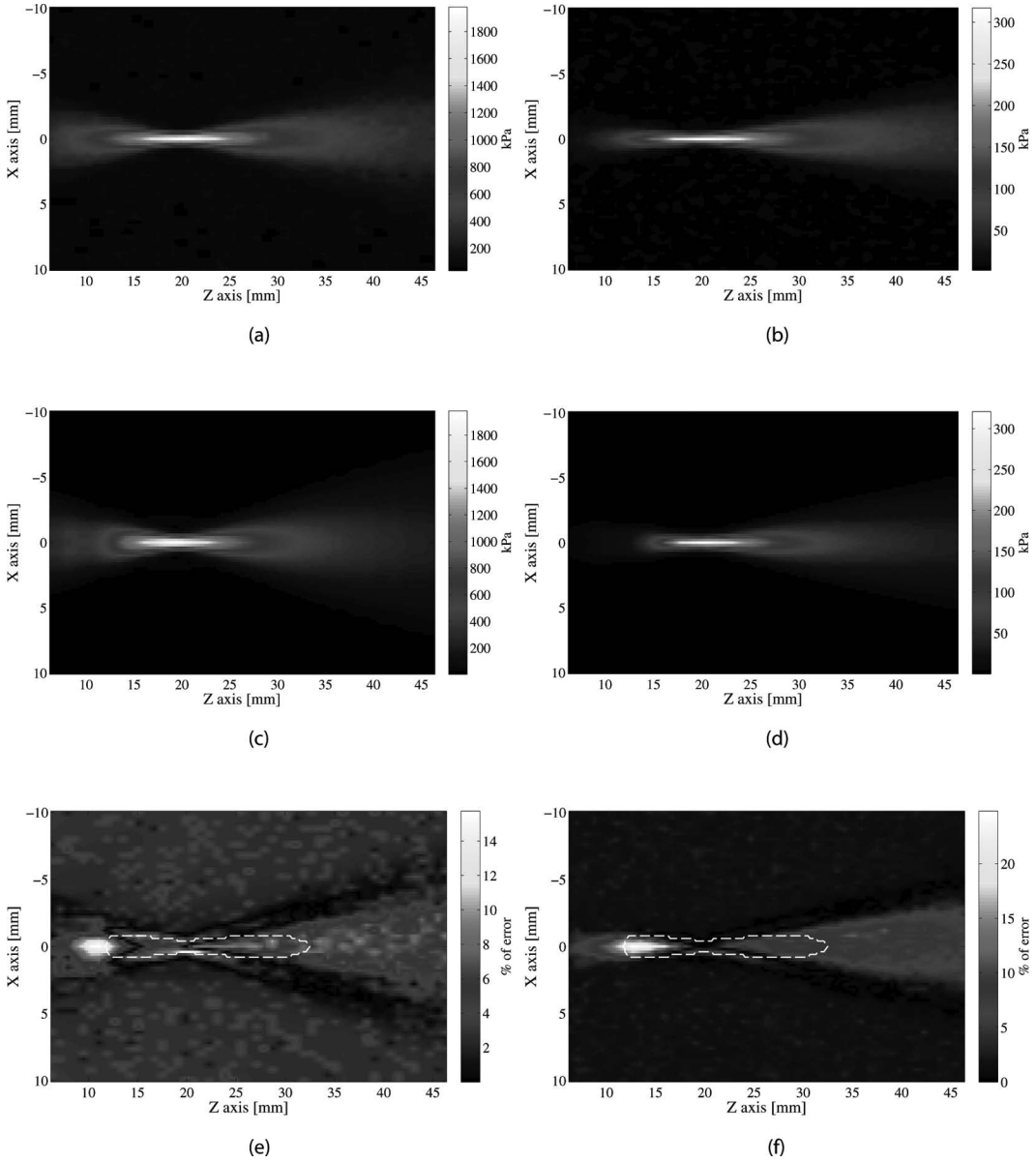

Fig. 7. Comparison of experimental focused beam (a) fundamental and (b) second harmonic and GASM simulated one-way fields for the (c) fundamental and (d) second harmonic. Error map of (e) the fundamental and (f) the second-harmonic component between the experimental field and GASM simulation. The dashed line is the −12-dB isoline.

β parameters perpendicular to the propagation direction but not on a layer juxtaposed parallel to the propagation axis. As shown in the examples in Fig. 5, the GASM can simulate the pressure field that propagates in media with arbitrary nonlinear parameter variations and could be adapted to the simulation of human tissues or of media containing contrast agents having a nonlinear parameter larger than the tissue [3]. As shown in Figs. 7 and 8, the GASM-simulated fundamental and second-harmonic fields are close to the experimental fields. The computation time of the GASM is about 13 times faster than standard nonlinear simulators. Faster nonlinear simulations of a complete 3-D space can be made. Of course, it must be remembered that the Voormolen simulator works for higher-order nonlinear interactions, whereas the GASM is based on first-order perturbation.

The GASM presents certain unavoidable limitations. First, the use of the FT adds noise in the resulting pressure field. This noise slightly degrades the final aspect of the field, although, as shown by the error maps, the accuracy of the GASM in the active part of the field is satisfactory. In the proposed approach, a compromise has been made between the accuracy and the speed of computation. An increase of the number of points considered in the different matrix will decrease the aliasing effect, but increases the computation time. For high-resolution simulations, tools based on the finite difference scheme, computing high-order nonlinear effects, must be preferred. Second, no nonlinear interactions between different frequency components are taken into account in the proposed simulator. Indeed, if a wave composed of two frequencies is transmitted in the

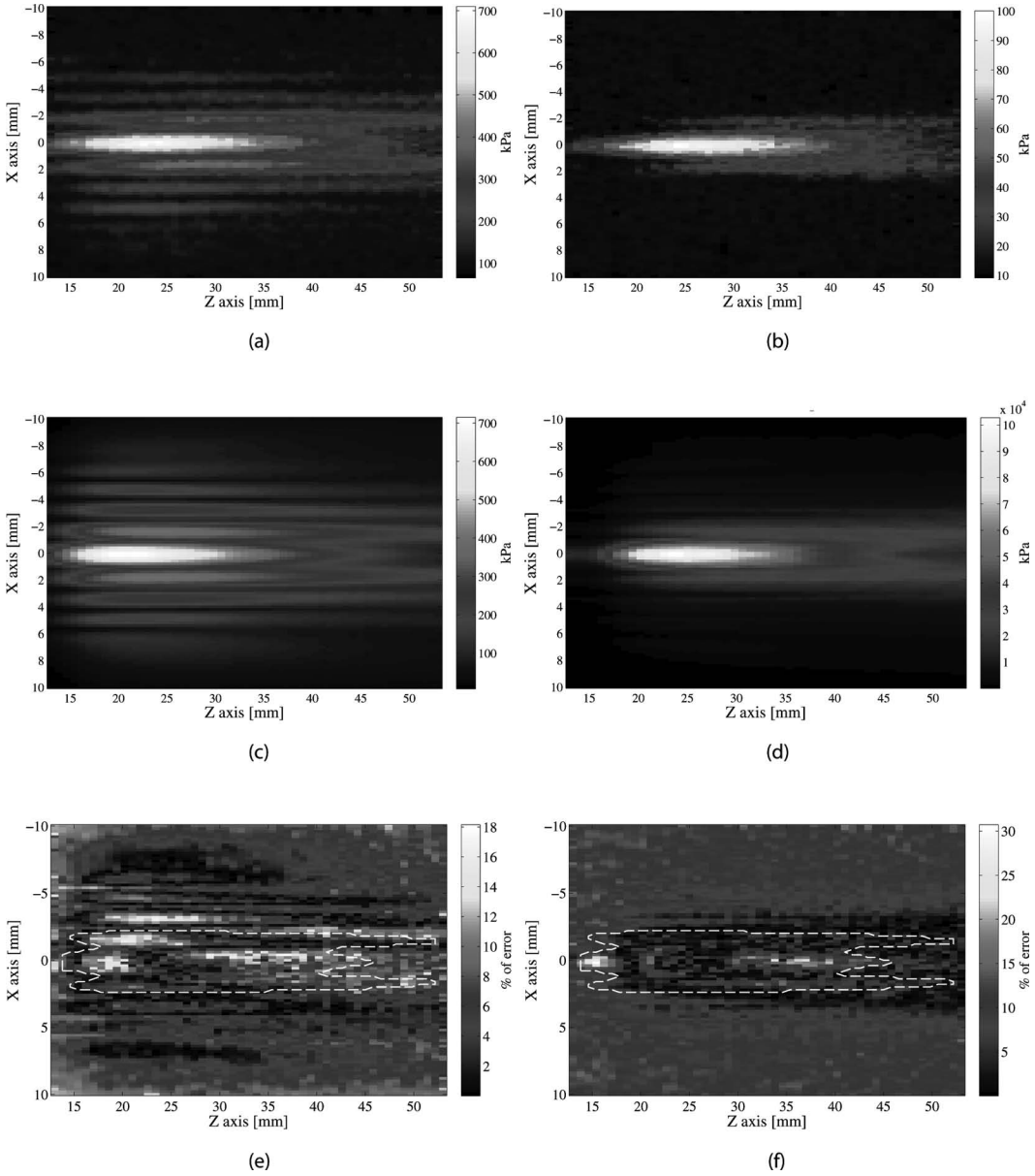

Fig. 8. Comparison of experimental unfocused beam (a) fundamental and (b) second harmonic and GASM simulated one-way fields for the (c) fundamental and (d) second harmonic. Error map of (e) the fundamental and (f) the second-harmonic component between the experimental field and GASM simulation. The dashed line is the −12-dB isoline.

medium, the simulator processes the wave as two single-frequency waves with no interactions between them. In a real medium, a nonlinear interaction takes place and creates other pressure waves at the difference and sum frequencies. Another limitation of the GASM is the quasi-linear approximation, which limits the simulation in terms of initial amplitude. If the second harmonic is not much smaller than the fundamental, this assumption is no longer valid and the nonlinearity phenomena are too large to be simulated with the GASM. This limit depends on the different probe parameters, on the beamforming in transmission, on the transmitted signal, and on the propagation depth to reach. The last approximation made in the proposed method consists of considering only transmitted waves and not taking into account any possible reflected waves caused by the inhomogeneous nonlinear map. This effect must be quantified in a future version of the GASM.

Future developments of this work would include the possibility of creating nonlinear RF images combining the GASM field simulation of a 3-D nonlinear parameter map with a 3-D scatterer map and a strategy in reception to reconstruct the RF image. Three-dimensional simulations of any application involving nonlinear imaging can be considered.

The GASM is currently usable for fundamental and second-harmonic computation. However, with the same quasi-linear approximation, a higher order of nonlinearity can be reached. The third- or fourth-harmonic can be simulated with an increase in computation time. An opti-

mal implementation must be found to relate the nonlinear order, the desired accuracy, and the computation time.

Appendix: Variation of the Constant

To solve (20), the variation of the constant technique is needed. First, the two characteristic solutions of (20) are

$$g_{1,2}(z) = e^{\pm iKz}. \tag{29}$$

To obtain the final solution of (20), the constant value of g_1 and g_2 must be computed. To do this, the two functions $\lambda_1(z)$ and $\lambda_2(z)$ must be calculated with

$$\lambda_1^{'}(z)g_1(z) + \lambda_2^{'}(z)g_2(z) = 0. \tag{30}$$

The system to be solved is

$$\begin{cases} \lambda_1(z)g_1(z) + \lambda_2(z)g_2(z) = g(z) \\ \lambda_1^{'}(z)g_1(z) + \lambda_2^{'}(z)g_2(z) = 0. \end{cases} \tag{31}$$

By deriving the first equation of (31) twice using the expression of g_1 and g_2, the system can be further developed:

$$\begin{cases} \lambda_1^{'}(z)g_1(z) + \lambda_2^{'}(z)g_2(z) = 0 \\ \lambda_1^{'}(z)g_1^{'}(z) + \lambda_2^{'}(z)g_2^{'}(z) = M(z). \end{cases} \tag{32}$$

Substitution of (29) into (32) leads to

$$\begin{cases} \lambda_1^{'}(z) = -\lambda_2^{'}(z)e^{-2iKz} \\ \lambda_1^{'}(z)(iK)e^{iKz} + \lambda_2^{'}(z)(-iK)e^{-iKz} = M(z). \end{cases} \tag{33}$$

Then, $\lambda_1^{'}(z)$ and $\lambda_2^{'}(z)$ can be extracted:

$$\begin{cases} \lambda_1^{'}(z) = -\frac{iM(z)}{2K}e^{-iKz} \\ \lambda_2^{'}(z) = \frac{iM(z)}{2K}e^{iKz}. \end{cases} \tag{34}$$

The final solution of (20) is given by

$$g(z) = \left(\int_{z_0}^{z} \lambda_1^{'}(u)\mathrm{d}u\right)e^{iKz} + \left(\int_{z_0}^{z} \lambda_2^{'}(u)\mathrm{d}u\right)e^{-iKz}. \tag{35}$$

References

[1] M. Averkiou, D. Roundhill, and J. Powers, "A new imaging technique based on the nonlinear properties of tissues," in *IEEE Ultrasonics Symp.*, 1997, vol. 2, pp. 1561–1566.

[2] X. Gong, D. Zhang, J. Liu, H. Wang, Y. Yan, and X. Xu, "Study of acoustic nonlinearity parameter imaging methods in reflection mode for biological tissues," *J. Acoust. Soc. Am.*, vol. 116, no. 3, pp. 1819–1825, 2004.

[3] J. Wu and J. Tong, "Measurements of the nonlinearity parameter B/A of contrast agents," *Ultrasound Med. Biol.*, vol. 24, no. 3, pp. 153–159, 1998.

[4] L. Bjørnø, "Forty years of nonlinear ultrasound," *Ultrasonics*, vol. 40, no. 1–8, pp. 11–17, 2002.

[5] V. Kuznetsov, "Equation of nonlinear acoustics," *Sov. Phys. Acoustics*, vol. 16, pp. 749–768, 1970.

[6] E. Zabolotskaya and R. Khokhlov, "Quasi-plane waves in the nonlinear acoustics of confined beams," *Sov. Phys. Acoustics*, vol. 15, pp. 35–40, 1969.

[7] P. Alais and P. Hennion, "Etude par une mthode de fourier de l'interaction non linaire de deux rayonnements acoustiques dans un milieu absorbant. Cas particulier de l'mission paramtrique," *Acustica*, vol. 43, no. 1, pp. 1–11, 1979. (in French)

[8] P. T. Christopher and K. J. Parker, "New approaches to nonlinear diffractive field propagation," *J. Acoust. Soc. Am.*, vol. 90, no. 1, pp. 488–499, 1991.

[9] P. T. Christopher and K. J. Parker, "New approaches to the linear propagation of acoustic fields," *J. Acoust. Soc. Am.*, vol. 90, no. 1, pp. 507–521, 1991.

[10] R. J. Zemp, J. Tavakkoli, and R. S. C. Cobbold, "Modeling of nonlinear ultrasound propagation in tissue from array transducers," *J. Acoust. Soc. Am.*, vol. 113, no. 1, pp. 139–152, 2003.

[11] J. Berntsen, "Numerical calculations of finite amplitude sound beams," in *Frontiers of Nonlinear Acoustics, 12th Int. Symp. Nonlinear Acoustics*, 1990, pp. 191–196.

[12] Y.-S. Lee and M. F. Hamilton, "Time-domain modeling of pulsed finite-amplitude sound beams," *J. Acoust. Soc. Am.*, vol. 97, no. 2, pp. 906–917, 1995.

[13] R. O. Cleveland, M. F. Hamilton, and D. T. Blackstock, "Time-domain modeling of finite-amplitude sound in relaxing fluids," *J. Acoust. Soc. Am.*, vol. 99, no. 6, pp. 3312–3318, 1996.

[14] M. M. Voormolen, "Three dimensional harmonic echocardiagraphy," Ph.D. dissertation, Dept. of Biomedical Engineering, Erasmus MC, Rotterdam, The Netherlands, 2007.

[15] T. Varslot and G. Taraldsen, "Computer simulation of forward wave propagation in soft tissue," *IEEE Trans. Ultrason. Ferroelectr. Freq. Control*, vol. 52, no. 9, pp. 1473–1482, 2005.

[16] T. Varslot and S.-E. Måsøy, "Forward propagation of acoustic pressure pulses in 3D soft biological tissue," *Model. Identif. Control*, vol. 27, no. 3, pp. 181–200, 2006.

[17] X. Yan, "Statistical model of beam distortion by tissue inhomogeneities in tissue harmonic imaging," Ph.D. dissertation, Dept. of Mechanical Engineering, The University of Texas at Austin, Austin, TX, 2004.

[18] J. Wojcik, A. Nowicki, P. A. Lewin, P. E. Bloomfield, T. Kujawska, and L. Filipczynski, "Wave envelopes method for description of nonlinear acoustic wave propagation," *Ultrasonics*, vol. 44, no. 3, pp. 310–329, 2006.

[19] S. I. Aanonsen, T. Barkve, J. N. Tjotta, and S. Tjotta, "Distortion and harmonic generation in the nearfield of a finite amplitude sound beam," *J. Acoust. Soc. Am.*, vol. 75, no. 3, pp. 749–768, 1984.

[20] M. F. Hamilton and D. T. Blackstock, "On the coefficient of nonlinearity beta in nonlinear acoustics," *J. Acoust. Soc. Am.*, vol. 83, no. 1, pp. 74–77, 1988.

[21] S. Dursun, T. Varslot, T. Johansen, B. Angelsen, and H. Torp, "Fast 3D simulation of 2nd harmonic ultrasound field from arbitrary transducer geometries," in *IEEE Ultrasonics Symp.*, 2005, vol. 4, pp. 1964–1967.

[22] D. Belgroune, J. F. de Belleval, and H. Djelouah, "Modelling of the ultrasonic field by the angular spectrum method in presence of interface," *Ultrasonics*, vol. 40, no. 1–8, pp. 297–302, 2002.

[23] Y. Du and J. Jensen, "Feasibility of non-linear simulation for Field II using an angular spectrum approach," in *IEEE Ultrasonics Symp.*, 2008, pp. 1314–1317.

[24] T. L. Szabo, "Generalized fourier transform diffraction theory for parabolically anisotropic media," *J. Acoust. Soc. Am.*, vol. 63, no. 1, pp. 28–34, 1978.

[25] J. Wojcik, "Conservation of energy and absorption in acoustic fields for linear and nonlinear propagation," *J. Acoust. Soc. Am.*, vol. 104, no. 5, pp. 2654–2663, 1998.

[26] M. Frigo and S. Johnson, "The design and implementation of fftw3," *Proc. IEEE*, vol. 93, no. 2, pp. 216–231, 2005.

[27] J. A. Jensen and N. B. Svendsen, "Calculation of pressure fields from arbitrarily shaped, apodized, and excited ultrasound transducers," *IEEE Trans. Ultrason. Ferroelectr. Freq. Control*, vol. 39, no. 2, pp. 262–267, 1992.

[28] J. A. Jensen, "Field: A program for simulating ultrasound systems," *Med. Biol. Eng. Comput.*, vol. 34, suppl. 1, pp. 351–353, 1996.

[29] J. Y. Lu, "Designing limited diffraction beams," *IEEE Trans. Ultrason. Ferroelectr. Freq. Control*, vol. 44, no. 1, pp. 181–193, 1997.

[30] P. Tortoli, L. Bassi, E. Boni, A. Dallai, F. Guidi, and S. Ricci, "Ula-op: an advanced open platform for ultrasound research," *IEEE Trans. Ultrason. Ferroelectr. Freq. Control*, vol. 56, no. 10, pp. 2207–2216, 2009.

François Varray was born in Montpellier, France, in 1985. He obtained his Engineering Diploma from the Ecole des Mines de Saint Etienne, France, in 2008, coupled with a master degree in image and signal processing. Since October 2008, he has worked for CREATIS, Lyon, France, and the Microelectronics Systems Design Lab, Firenze, Italy, as a Ph.D. student. His main research interests concern nonlinear ultrasound propagation simulation, nonlinear image simulation, and nonlinear parameter imaging.

Alessandro Ramalli was born in Prato, Italy, in 1983. He received a Bachelor's degree in electronic engineering in 2006 and a Master's degree in electronic engineering in 2008 from the University of Florence, Italy. Since 2009, he has been working as a Ph.D. student in co-agreement between the Microelectronics Systems Design Laboratory (MSD-Lab), Florence, and the Centre de Recherche en Acquisition et Traitement de l'Image pour la Santé (CREATIS), Lyon. His research interests include ultrasound high frame-rate imaging, elastography, and Doppler application.

Christian Cachard received his Ph.D. in acoustics from INSA-Lyon in 1988, in the field of signal processing for underwater acoustics. He is now a Professor at the Electrical Department of the Technical Institute Université Lyon 1 Claude Bernard. Since he joined the research laboratory CREATIS, his domain of interest includes ultrasound medical imaging, ultrasound contrast agent imaging, ultrasound radio frequency processing, and microtools localization in 3-D ultrasound data.

Piero Tortoli (M'91–SM'96) received the Laurea degree in electronics engineering from the University of Florence, Italy, in 1978. Since then, he has been with the Electronics and Telecommunications Department of the University of Florence, where he is currently a full professor of Electronics and Department Head. Piero has been a member of the IEEE International Ultrasonics Symposium Technical Program Committee since 1999. He organized the 22nd International Symposium on Acoustical Imaging (1995), the 12th New England Doppler Conference (2003), and the Artimino Conference on Medical Ultrasound Technology (2011). In 2000, he was nominated to be an Honorary Member of the Polish Academy of Sciences. His research activity is centered on the development of ultrasound research systems and novel imaging/Doppler methods.

Olivier Basset was born in Bourg en Bresse, France, in 1963. He received, in 1986, the M.S. degree in biomedical engineering from the National Institute of Applied Sciences of Lyon and University Lyon I, France. He received the Ph.D. degree in Signal and Image Processing in Acoustics from the National Institute of Applied Sciences in Lyon, in 1991. He is currently a Professor in the University Claude Bernard-Lyon I.

He is a member of CREATIS Laboratory (CNRS 5220, INSERM U1044). His research interests concern ultrasonic image processing: elastography, tissue characterization, and nonlinear imaging.